In Vitro Cytotoxic Performance of Pure and Co-Doped CeO_2 Nanoparticles on Breast Cancer Cell, Colon Cancer Cell, and Mouse Embryo Fibroblast Cell Lines

Abdolhossein Miri
Mina Sarani (minasarani64@gmail.com)
https://orcid.org/0000-0002-0681-0421
Mahmood Barani
Rajender S. Varma
Mohammad Javad Miri

Research Article

Keywords: Co-doped CeO2 NPs, B. multifidi, breast cell line, CaCo2 cells, NIH-3T3 cells

Posted Date: February 2nd, 2022

DOI: https://doi.org/10.21203/rs.3.rs-1300456/v1

Abstract

Today, according to the progression and prevalence of cancer, efforts to discover new compounds to suppress the tumor and associated with less toxicity. Metal oxide nanoparticles have wide applications in biology and biomedicine due to their unique physical and chemical properties. They have great potential in the treatment of cancer, tumor targeting in tissues, targeted drug delivery, bioimaging, gene therapy and other diagnostic and therapeutic areas. So, in this study, a simple, inexpensive, and environmentally friendly method is described for the pure and 1, 4, and 8% cobalt doped cerium oxide nanoparticles (Co-doped CeO_2 NPs) using aqueous extract of *Biebersteinia multifidi* roots, as a recommended compound for the treatment of cancer. The morphology and size of synthesized nanoparticles were determined using PXRD, UV-Vis, FESEM, EDX, and Raman methods wherein cobalt doped cerium oxide were identified as spherical in shape with an average size of 5-10 nm. The toxicity effect of synthesized pure and Co-doped CeO_2 NPs on breast cancer cell (MCF7), colon cancer cell (CaCo2), and mouse embryo fibroblast cell (NIH-3T3) lines was examined using MTT assay; cerium oxide nanoparticles were non-toxic against cancer and normal cell lines while Co-doped CeO_2 NPs displayed cytotoxic effects on MCF7 and CaCo2 cell lines, except for NIH-3T3 cell line compared to doxorubicin as control. Thus, synthesized Co-doped CeO_2 NPs have shown an acceptable inhibitory effect on breast and colon cancer cell lines.

1 Introduction

Nanotechnology, among emerging technologies, deals with structures of nano size (1 to 100 nm scale) and have innumerable novel and beneficial attributes as established by many researchers worldwide [1–3]. The wide-ranging technological appliances in the field of electronics, imaging, industrial, and health, among others include diagnostics, treatment, and new drug formulations in view of their unique and specific physico-chemical properties, thus embracing various disciplines namely physics, biological, and chemistry [4].

Cerium oxide nanoparticles, comprising cerium atoms surrounded by oxygen networks, have been widely deployed in polishing of mechanical chemical, solar cells, fuel oxidation analytical, corrosion protection, and automobile exhaust treatment. These nanoparticles also show imitation of superoxide dismutase, peroxidase, catalase, phosphatase activity and the inhibition of hydroxyl radical, proxy nitrite, and nitric oxide radicals [5].

A few studies have indicated the oxidative stress induction caused by nanoceria in vitro and in vivo where nanoceria has directly functioned as an antioxidant, and served as free radical scavenger as well; they interact with superoxide radical, hydroxyl and peroxide radical, and thus leading to cell death due to oxidative stress [5–7]. Consequently, CeO_2 NPs can be utilized as potential drug agents in pharmacy setting, and biological scaffolding [8–10], the basis for these activities being the redox cycles between +3 and +4 states, and their specific ability in adsorption and released of oxygen [11, 12]. Although initially believed that both, the oxygen vacancy and redox cycles between these two states of cerium is involved in antioxidant activity, but now it has been accepted that redox cycle is primarily responsible for all the

antioxidant properties [12, 13]; surface ratio of Ce^{+3}/Ce^{+4} plays a key role in most of the biological activities of CeO_2 NPs [14]. CeO_2 NPs also serve as oxidant at low pH and high doses, and based on synthesis method, concentration, and exposure time may have potentially cytotoxic function [15]. So, careful optimization of appropriate synthetic parameters can produce relatively non-toxic CeO_2 NPs, with oxidant or antioxidant properties [5].

The physico-chemical property of nanoparticles is determined largely by variation in synthetic methods which prompts us to explore the generation of CeO_2 NPs with different size, morphology and aggregation. Recently, bio-inspired biological methods as stabilizing agents have garnered importance in the production of CeO_2 NPs, because of the reduced concerns regarding their biocompatibility. Adhering to the green chemistry principles [16] has provided safer routes for the production of CeO_2 NPs, which can be useful for drug applications; indeed, these methods offer cheaper and simpler options than the traditional chemical synthetic methods [17–21]. Another important factor for effective and important nanoparticles properties is the doping process as attested by several studies wherein the properties of doped nanoparticles with various metals have dramatic alterations compared to un-doped nanoparticles; synthetic methods for doped nanoparticles being similar [22–24].

Biebersteinia multifida is a perennial herbaceous plant with thick roots and stems with numerous longitudinal grooves that are covered with tuberous protrusions. This plant grows in many forms in Iran, Syria, Lebanon, Armenia, Central Asia, and Afghanistan and contains various alkaloids. The roots of this plant contain carbohydrates, saponins, flavonoids, and biopolymers such as monosaccharides, starches and dextrins while the aerial parts comprise triterpene saponins, essential oils, alkaloids and tannins [25]. Herein, pure and cobalt doped cerium oxide nanoparticles were synthesized using *B. multifida* aqueous extract, and their cytotoxic effects were assessed on breast cancer cell (MCF7), colon cancer cell (CaCo2), and mouse embryo fibroblast cell (NIH-3T3) lines.

2 Experimental

2.1 Synthesis of pure and Co-doped CeO_2 NPs

The extract from *B. multifidi* was deployed for the synthesis of nanoparticles. For this purpose, *B. multifidi* roots was washed, dried, and crushed. 10 gr of plant powder was dissolved in 100 mL of distilled water (1:10 ratio) and it was shaken at 150 rpm at 24 hours. Then this mixture was filtered using Whatman 1 filter paper. Next, 10 mL of extract was diluted with 50 mL of distilled water. Then 50 mL of $Ce(NO_3)_3.6H_2O$ (0.02 M) was added along with $Co(SO_4).7H_2O$ (in ratios of 0, 1, 4, and 8 w/w, separately) to extract solution, and these were placed in water bath at a 70°C for 3 hours. Subsequently, after centrifuged, solutions were dried in an oven (90°C), and the ensuing residue was calcined using a digital furnace at 400°C temperature for 2 hours.

2.2 Characterization

The Powder X-ray diffraction (PXRD) spectra for the prepared nanoparticles were determined using the employment of X-ray diffraction model X'Pert PRO MPD PANalytical Company (Netherlands Formation), while their morphology was identified through the usage of scanning electron microscopy (SEM), TESCAN model MIRA3. Raman spectra were captured deploying a Raman Takram P50C0R10 at a wavelength of 532 nm. The electronic adsorption of prepared nanoparticles was realized by an UV-Vis spectrophotometer model 1800 made by Shimadzo Japan.

2.3 Cytotoxic activity

2.3.1 Cell culture

Cell lines of CaCo2 (colon cancer cells), MCF-7 (breast cancer cells), and NIH-3T3 (mouse embryo fibroblast cells) were purchased from the Iranian Biological Resource Center (IBRC, Tehran, Iran) and cultured in 25 mL flasks containing DMEM and 10% (v/v) FBS and 10 µL/mL penicillin-streptomycin antibiotics. Then, cells were seeded separately into 96 multi-well plates at a density of 10×10^3 cells per well at 37°C for 24 h to reach confluences. The cells were treated with varying concentrations of nanoparticle (1–1000 µg/mL) for 24 hours; Doxorubicin was used as a positive control. Following the treatment, 10 µL of MTT reagent was added into each well and incubated for an additional 4 h at 37°C in the darkness. After incubation, the medium was removed and 100 µL DMSO added to each well. The formation of formazan was recorded by reading absorbance at a wavelength of 570 nm using a microplate reader (Bio-Tek ELX800, USA). The viable cell percentages were presented for the vehicle-treated group.

2.3.2 MTT assay

Cell lines (CaCo2, MCF-7, and NIH-3T3) were seeded separately into 96 multi-well plates at a density of 10×10^3 cells per well at 37°C for 24 h to reach confluences. Then, the cells were treated at different concentrations of nanoparticle (1–1000 µg/mL) for 24 hours; Doxorubicin was used as the positive control. Following the treatment, 10 µL of MTT reagent was added into each well and incubated for an additional 4 h at 37°C in the darkness. After incubation, the medium was removed and 100 µL DMSO was added to each well. The formation of formazan was recorded by reading absorbance at a wavelength of 570 nm using a microplate reader (Bio-Tek ELX800, USA). The viable cell percentages were presented for the vehicle-treated group.

3 Results And Discussion

3.1 PXRD analysis

PXRD spectra of pure and 1, 4, and 8% Co-doped CeO_2 NPs are depicted in Figure 1, which determined crystalline properties of synthesized nanoparticles. As seen in Fig. 1, the four peaks appeared in regions of 43.47, 72. 32, 41.28, 56.43° accordance with (111), (200), (220), and (311) levels, which indicated on face-centered cubic (FCC) structure for the synthesized nanoparticles (JCPDS: 00-043-1002). With doped

cobalt to the crystalline structure of cerium oxide was observed a slight change in (111) peak, which represents the entry of cobalt into the crystal structure of cerium oxide nanoparticles. This change may be due to differences in the ionic radii of cobalt and cerium atoms, as ionic radius of $Co^{+2/+3}$ (0.75-0.9 Å) is lesser than to ionic radius of Ce^{+4} (0.97 Å). Figure 1, the peaks widened with an increase of doped cobalt percentage, which can be due to the decrease of particle size (Figure 1). Using Debye-Scherrer [18] equation, obtained data from PXRD spectra revealed the estimated crystalline size of synthesized nanoparticles. The crystalline size of pure, 1%, 4%, and 8% Co-doped CeO_2 nanoparticles was obtained 9.64, 9.68, 7.42, and 6.23 nm, respectively; doped cobalt caused the reduction of the crystalline size of synthesized nanoparticles.

3.2 FESEM and EDX analysis

To understand accurately the shape and size, FESEM imaging was performed for the synthesized nanoparticles which for pure and 1%, 4%, and 8% Co-doped CeO_2 NPs are depicted in Figure 2. The size of the CeO_2 NPs was less than 10 nm, but after the cobalt doping, the size of these nanoparticles became smaller. According to the atomic radius of cobalt (125 pm) and cerium (181.5 pm), it can be assumed that with increasing concentration of doped cobalt in the crystal structure of cerium oxide particles, their size decreases. Based on EDX images of synthesized nanoparticles (Figure 3), cobalt has clearly entered into the structure of cerium oxide and that they are pure. The percentage of Ce atom was determined to be 77.79, 75.56, and 60.45% and Co atom is 0.89, 3.71, and 7.46% in 1%, 4%, and 8% Co-doped CeO_2 NPs.

3.3 Raman analysis

Raman spectroscopy is an important tool for analyzing the phase purity, structural defects, and some disorders such as oxygen deficiency in synthesized samples. As shown in Figure 4, the band in region 458 cm^{-1} indicates the F2g state of the cube fluoride structure of cerium oxide, which can be attributed to the state of Ce-O8 symmetric vibration. Due to the individual motion of the oxygen atoms, the vibrational state is almost dependent on the mass of the cation. In doped cerium oxide nanoparticles with 1, 4, and 8% cobalt, this band appeared in the region of 446, 446, and 440 cm^{-1}, respectively. It has been confirmed that this band can be transferred to lower regions using increasing the concentration of doped cobalt to cerium oxide, due to created oxygen deficiency with the entry of cobalt cation into the crystal structure of cerium oxide [23, 26]. In addition, the particle size factor can also influence the position of this band as it has been observed that the F2g mode has been shifted to lower regions due to the reduction in particle size [23].

3.4 UV-Vis analysis

Ultraviolet (UV-Vis) spectroscopy of material is observed throughout the UV region due to its absorption in electromagnetic radiation which provides valuable qualitative and especially quantitative information for the sample (Figure 5). The electron spectrum of CeO_2 NPs has a peak at 309 cm^{-1}, while peaks of doped CeO_2 NPs with 1, 4, and 8% cobalt were observed in the regions at 333, 329, and 253 cm^{-1}, respectively. Doping of cobalt in the crystal structure CeO_2 NPs has led to a change in its electron spectrum towards

shorter wavelengths, which could be due to the electron transfer of doped cobalt in the cubic structure of these nanoparticles [23].

3.5 Cytotoxic performance

Cell proliferation and cell viability are assessed by adding tetrazolium salts to the cell culture medium, tetrazolium salts being converted to formazan by cellular enzymes. The number of viable cells can be predicted based on the activity of mitochondrial dehydrogenase enzymes in the sample. If the activity of these enzymes is higher, the amount of produced formazan dye in the culture medium will increase, which directly indicates the number of metabolically active cells in the culture medium. To determine the number of active cells in the culture medium, formazan dye solution is absorbed in ELISA reader at appropriate wavelengths [19].

The generated cytotoxicity on breast cancer cells (MCF-7), colon cancer cells (CaCo2), and mouse embryo fibroblast cell (NIH-3T3) line using pure and 1, 4, and 8% cobalt doped nanoparticles was evaluated through the MTT test, and the results are shown in Figure 6. The calculated IC_{50} for synthesized nanoparticles and doxorubicin as control is shown in Table 1. In Figure 7, the cell images were depicted before and after treatment with 8% Co doped CeO_2 NPs again MCF-7, CaCo2, and NIH-3T3 cells.

Table 1
IC_{50} values of synthesized un-doped and Co-doped CeO_2 NPs using *B. multifidi* extract.

Cell line	IC_{50} of synthesized cerium oxide nanoparticles (µg/mL)				Control
	pure	1% doped Co	4% doped Co	8% doped Co	Doxorubicin
CaCo2	1172	1192	776.9	171.2	110.1
MCF-7	1316	1252	963.3	227.4	186.9
NIH-3T3	2140	7900	21043	11640	759

As shown in Figure 6, CeO_2 NPs are nontoxic against CaCo2 and MCF-7 cell lines, but after cobalt doping CeO_2 NPs displayed enhanced cytotoxic effect on breast and colon cancer cell lines; for 8% Co-doped CeO_2 NPs, IC_{50} values obtained are 171.2 and 227.4 µg/mL for CaCo2 and MCF-7 cell lines, respectively, which is closer to IC_{50} of doxorubicin as control (Table 1). In case of NIH-3T3 cell line, however, doped nanoparticles have not displayed considerable cytotoxic effect. Of course, the CeO_2 NPs in high concentration (≤1000 µg/mL) show diminutive cytotoxic effect. This study shows the biocompatibility of green synthesized nanoparticles and agrees with the previous similar reports for other nanoparticles; green synthesized biogeneic approach as an alternate method that relies on natural organisms for the reduction of metal ions into stable and biocompatible NPs [27–29]. For example, Irshad *et al.* prepared CeO_2 NPs using orange peel extract (OPE) with considerable antioxidant activity [30]. In another study, Rajan et al. used fruit extract of Morus nigra for the fabrication of CeO_2 NPs and their cell viability studied using L929 cell lines, which affirmed its biocompatible nature [31].

4 Conclusion

Herein, pure, 1, 4, and 8% cobalt-doped cerium oxide nanoparticles were successfully prepared using root extract of *Biebersteinia multifidi*. The physicochemical properties of prepared nanoparticles were determined and analyzed wherein the results revealed that the synthesized nanoparticles are uniform and spherical in shape. The size of CeO_2 NPs is less 10 nm and with the addition of cobalt in the structure of nanoparticles, the size of nanoparticles has become smaller. Toxicity effect of synthesized nanoparticles on MCF-7, CaCo2, NIH-3T3 cancer cell lines was assessed through MTT assay which revealed that cerium oxide nanoparticles were non-toxic on three cell lines, but Co-doped CeO_2 NPs were toxic on MCF-7 and CaCo2 cells. Also, increasing the percentage of cobalt in the structure of cerium oxide increased the cytotoxicity in these cells. Thus, the synthesized nanoparticles can be used for the cancer treatment and related biological applications such as drug delivery, among other formulations.

Declarations

Conflict of interest

The authors declare that they have no conflict of interest.

References

1. E.N. Zare, X. Zheng, P. Makvandi, H. Gheybi, R. Sartorius, C.K. Yiu, M. Adeli, A. Wu, A. Zarrabi, R.S. Varma, Small **17**, 2007073 (2021)
2. S. Iravani, R.S. Varma, Environm. Chem. Lett **18**, 703–727 (2020)
3. M. Barani, M. Mukhtar, A. Rahdar, S. Sargazi, S. Pandey, M. Kang, Biosensor **11**, 55 (2021)
4. M. Nadeem, R. Khan, K. Afridi, A. Nadhman, S. Ullah, S. Faisal, Z.U. Mabood, C. Hano, B.H. Abbasi, Int. J. Nanomed. **15**, 5951 (2020)
5. A. Dhall, W. Self, Antioxidant **7**, 97 (2018)
6. R. Arshad, M. Barani, A. Rahdar, S. Sargazi, M. Cucchiarini, S. Pandey, M. Kang, Biosensor **11**, 97 (2021)
7. F. Sabir, M. Qindeel, M. Zeeshan, Q. Ul Ain, A. Rahdar, M. Barani, E. González, M.A. Aboudzadeh, Processe **9**, 621 (2021)
8. M. Li, P. Shi, C. Xu, J. Ren, X. Qu, Chem. Sci **4**, 2536–2542 (2013)
9. J.A. Vassie, J.M. Whitelock, M.S. Lord, Mol. Pharm **15**, 994–1004 (2018)
10. C. Mandoli, F. Pagliari, S. Pagliari, G. Forte, P. Di Nardo, S. Licoccia, E. Traversa, Adv. Func. Mater **20**, 1617–1624 (2010)
11. S. Deshpande, S. Patil, S.V. Kuchibhatla, S. Seal, App. Phys. Lett **87**, 133113 (2005)
12. C. Korsvik, S. Patil, S. Seal, W.T. Self, Chem. Commun 1056-1058 (2007)
13. V.K. Ivanov, A.B. Shcherbakov, A. Usatenko, Russ. Chem. Rev. **78**, 855 (2009)

14. I. Celardo, M. De Nicola, C. Mandoli, J.Z. Pedersen, E. Traversa, L. Ghibelli, ACS Nano **5**, 4537–4549 (2011)
15. R.A. Yokel, S. Hussain, S. Garantziotis, P. Demokritou, V. Castranova, F.R. Cassee, Environm. Sci. Nano **1**, 406–428 (2014)
16. R.S. Varma, Curr. Opin. Chem. Eng **1**, 123–128 (2012)
17. M. Darroudi, M. Sarani, R.K. Oskuee, A.K. Zak, H.A. Hosseini, L. Gholami, Ceram. Int. **40**, 2041–2045 (2014)
18. A. Miri, H. Beiki, A. Najafidoust, M. Khatami, M. Sarani, Bioproc. Biosysts. Eng 1-9 (2021)
19. A. Miri, S. Akbarpour Birjandi, M. Sarani, J. Biochem. Mol. Toxic **34**, e22475 (2020)
20. R.S. Varma, ACS Public **4**(11), 5866–5878 (2016)
21. R.S. Varma, Green Chem. **16**, 2027–2041 (2014)
22. A. Miri, M. Sarani, M. Khatami, Rsc Adv **10**, 3967–3977 (2020)
23. K. Hamidian, A. Najafidoust, A. Miri, M. Sarani, Mater. Res. Bull **138**, 111206 (2021)
24. K. Hamidian, M.R. Saberian, A. Miri, F. Sharifi, M. Sarani, Ceram. Int. **47**, 13895–13902 (2021)
25. A. Miri, S.R. Mousavi, M. Sarani, Z. Mahmoodi, Orien. J. Chem **34**, 1513 (2018)
26. V. Fernandes, J. Klein, oN. Mattoso, D. Mosca, E. Silveira, E. Ribeiro, W. Schreiner, J. Varalda, A. de Oliveira, Phys. Rev. B **75**, 121304 (2007)
27. M. Ahamed, M.M. Khan, M. Siddiqui, M.S. AlSalhi, S.A. Alrokayan, Phys. E.: Low-dimen. Syst. Nanostr. **43**, 1266–1271 (2011)
28. G. Von White, P. Kerscher, R.M. Brown, J.D. Morella, W. McAllister, D. Dean, C.L. Kitchens, J. Nanomateri 2012, (2012)
29. P. Mukherjee, A. Ahmad, D. Mandal, S. Senapati, S.R. Sainkar, M.I. Khan, R. Ramani, R. Parischa, P. Ajayakumar, M. Alam, Angew. Chem. Int. Edi **40**, 3585–3588 (2001)
30. M.S. Irshad, M.H. Aziz, M. Fatima, S.U. Rehman, M. Idrees, S. Rana, F. Shaheen, A. Ahmed, M.Q. Javed, Q. Huang, Mater. Res. Exp **6**, 0950a0954 (2019)
31. A.R. Rajan, V. Vilas, A. Rajan, A. John, D. Philip, Ceram. Int. **46**, 14048–14055 (2020)

Figures

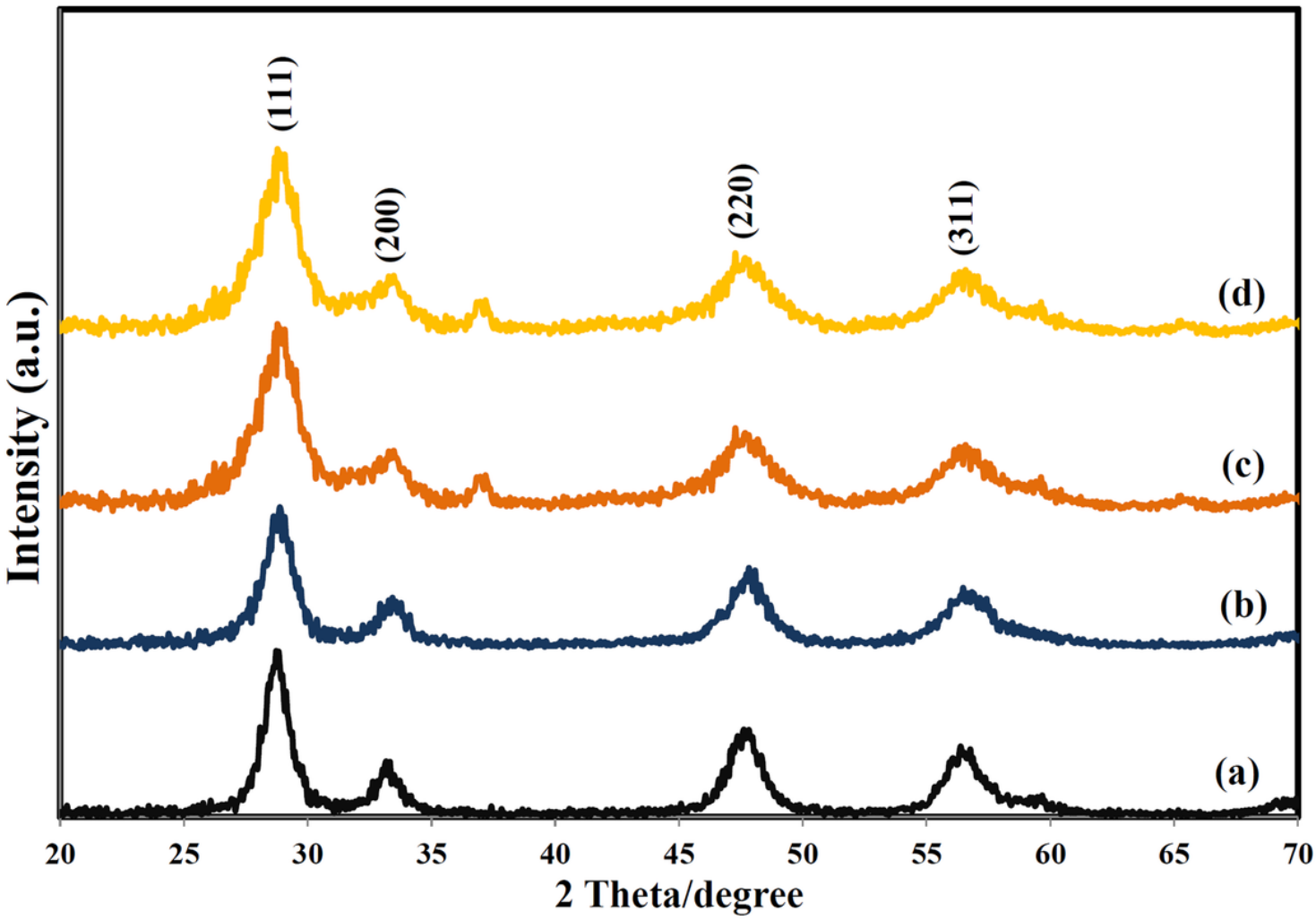

Figure 1

PXRD spectra of synthesized (a) pure, (b) 1% Co-doped, (c) 4% Co-doped, and (d) 8% Co-doped CeO_2 NPs using *B. multifidi* extract.

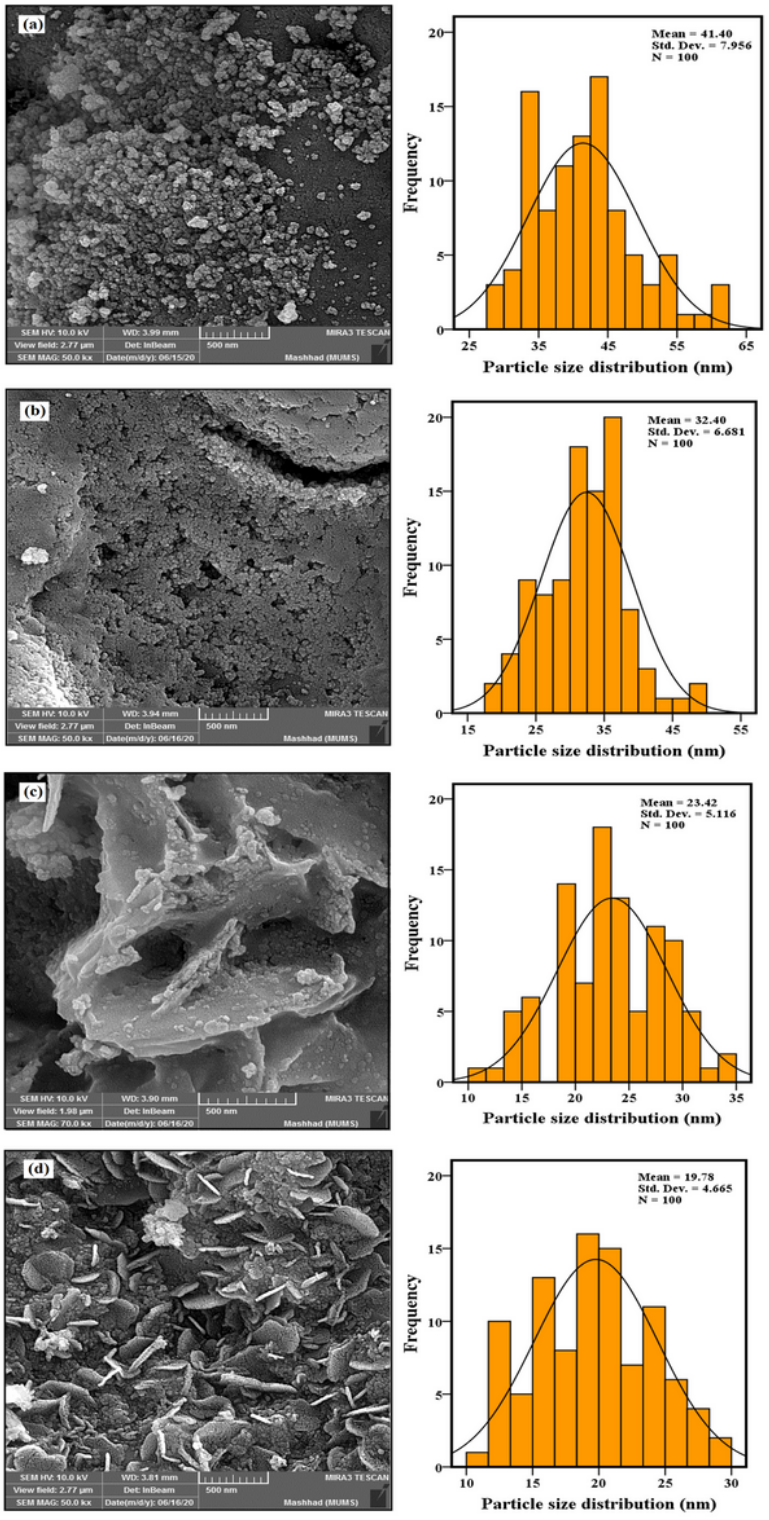

Figure 2

FESEM images of synthesized (a) pure, (b) 1% Co-doped, (c) 4% Co-doped, and (d) 8% Co-doped CeO_2 NPs using *B. multifidi* extract.

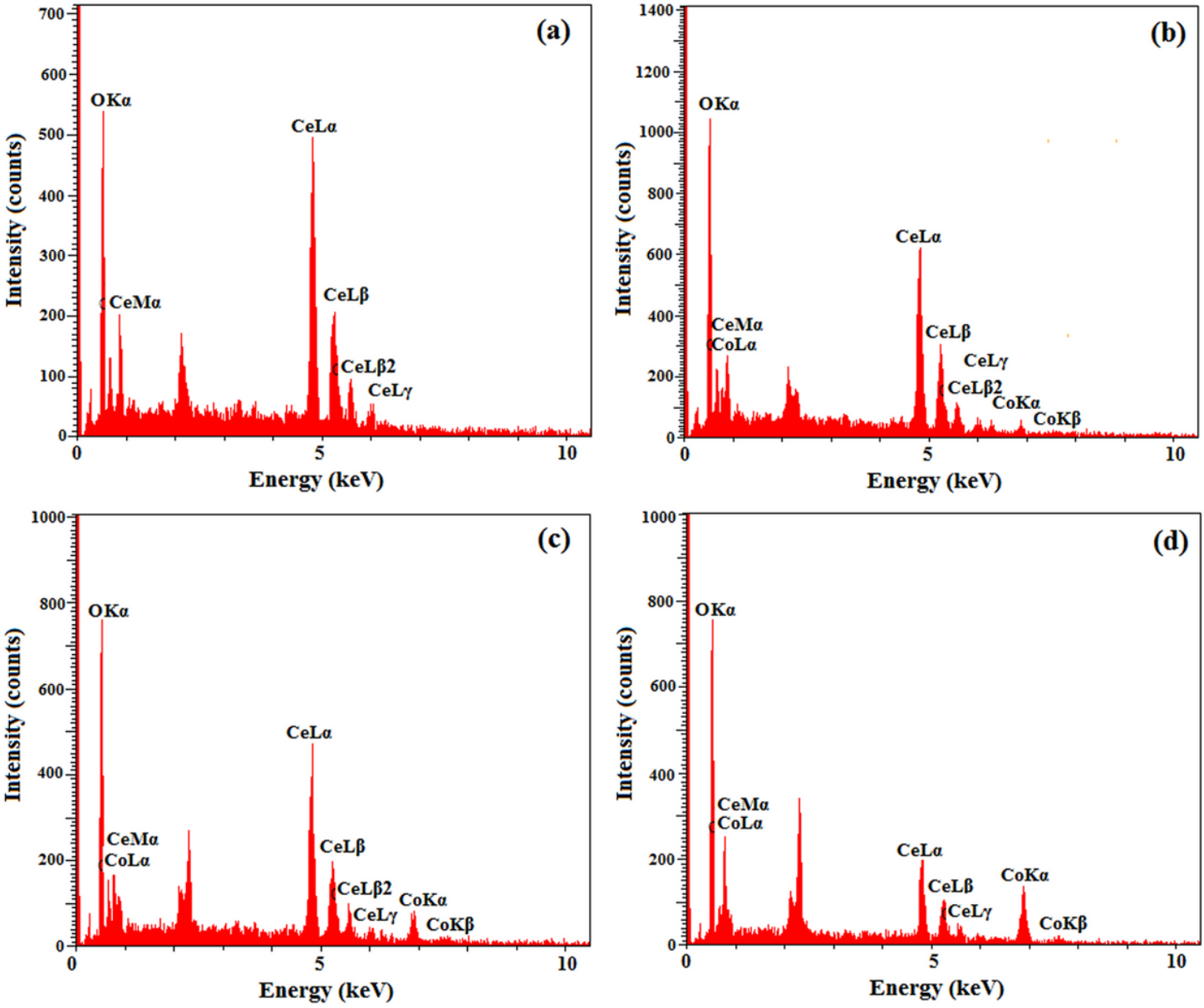

Figure 3

EDX spectra of synthesized (a) pure, (b) 1% Co-doped, (c) 4% Co-doped, and (d) 8% Co-doped CeO_2 NPs using *B. multifidi* extract.

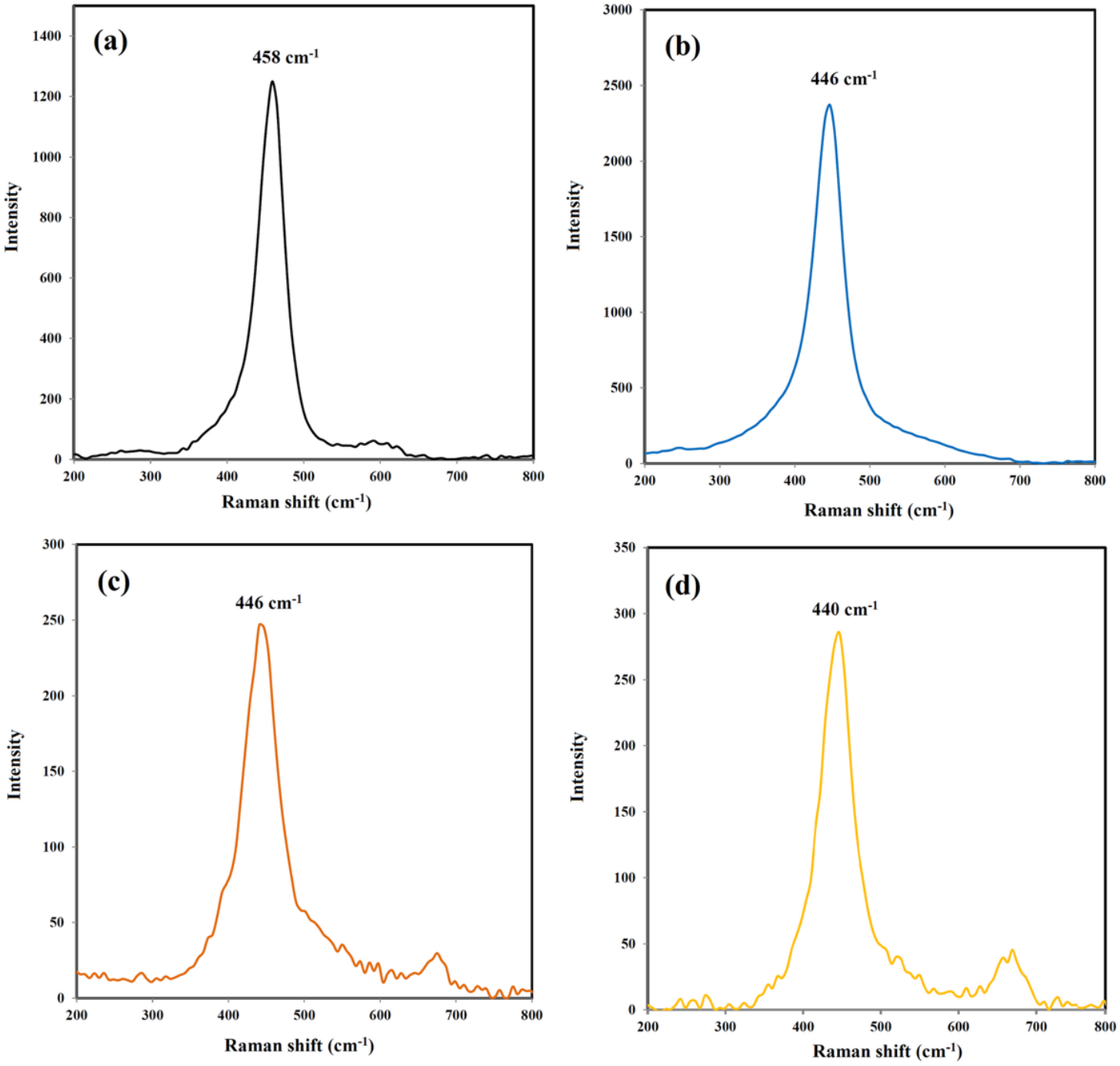

Figure 4

Raman spectra of synthesized (a) pure, (b) 1% Co-doped, (c) 4% Co-doped, and (d) 8% Co-doped CeO_2 NPs using *B. multifidi* extract.

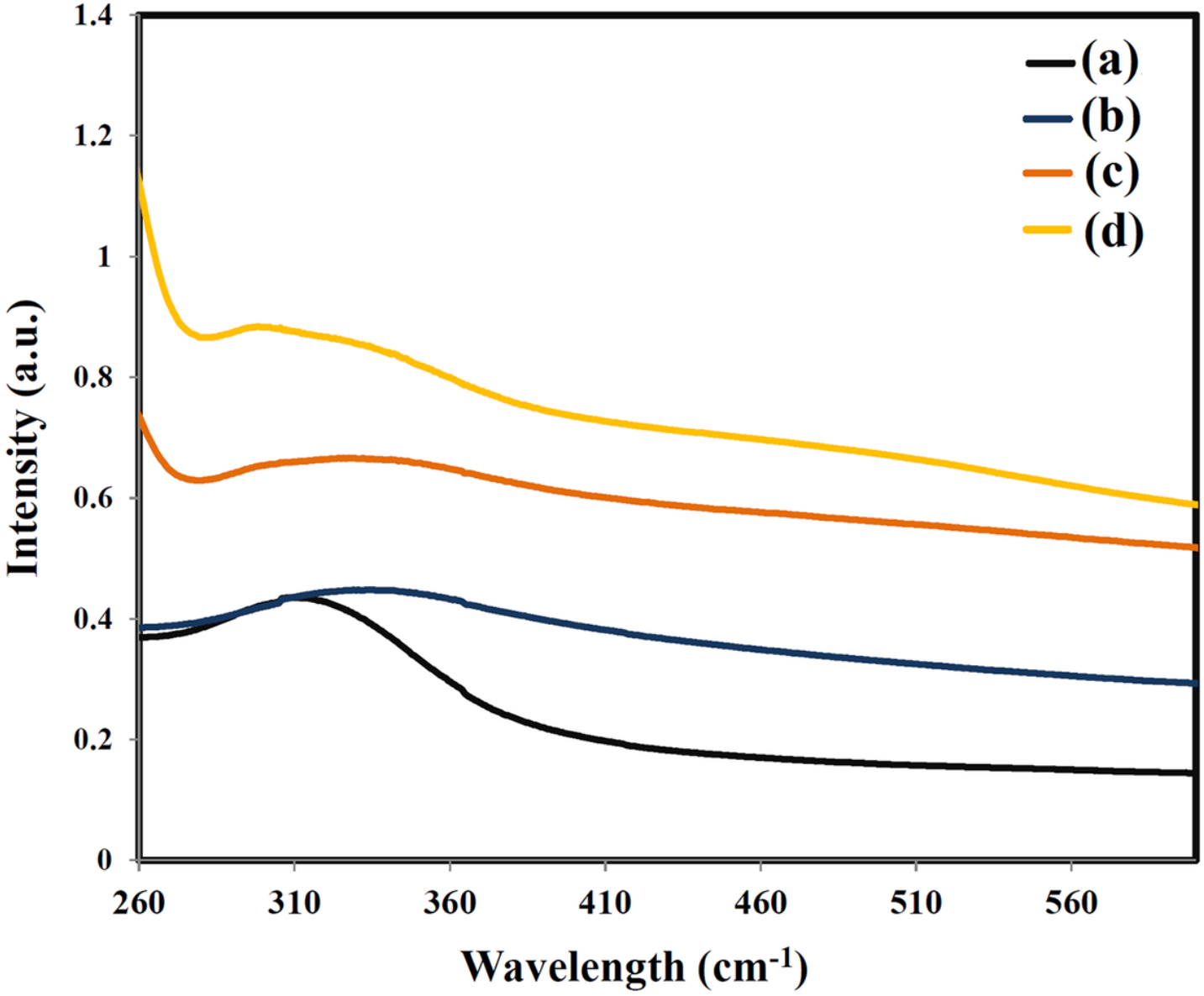

Figure 5

UV-Vis spectra of synthesized (a) pure, (b) 1% Co-doped, (c) 4% Co-doped, and (d) 8% Co-doped CeO_2 NPs using *B. multifidi* extract.

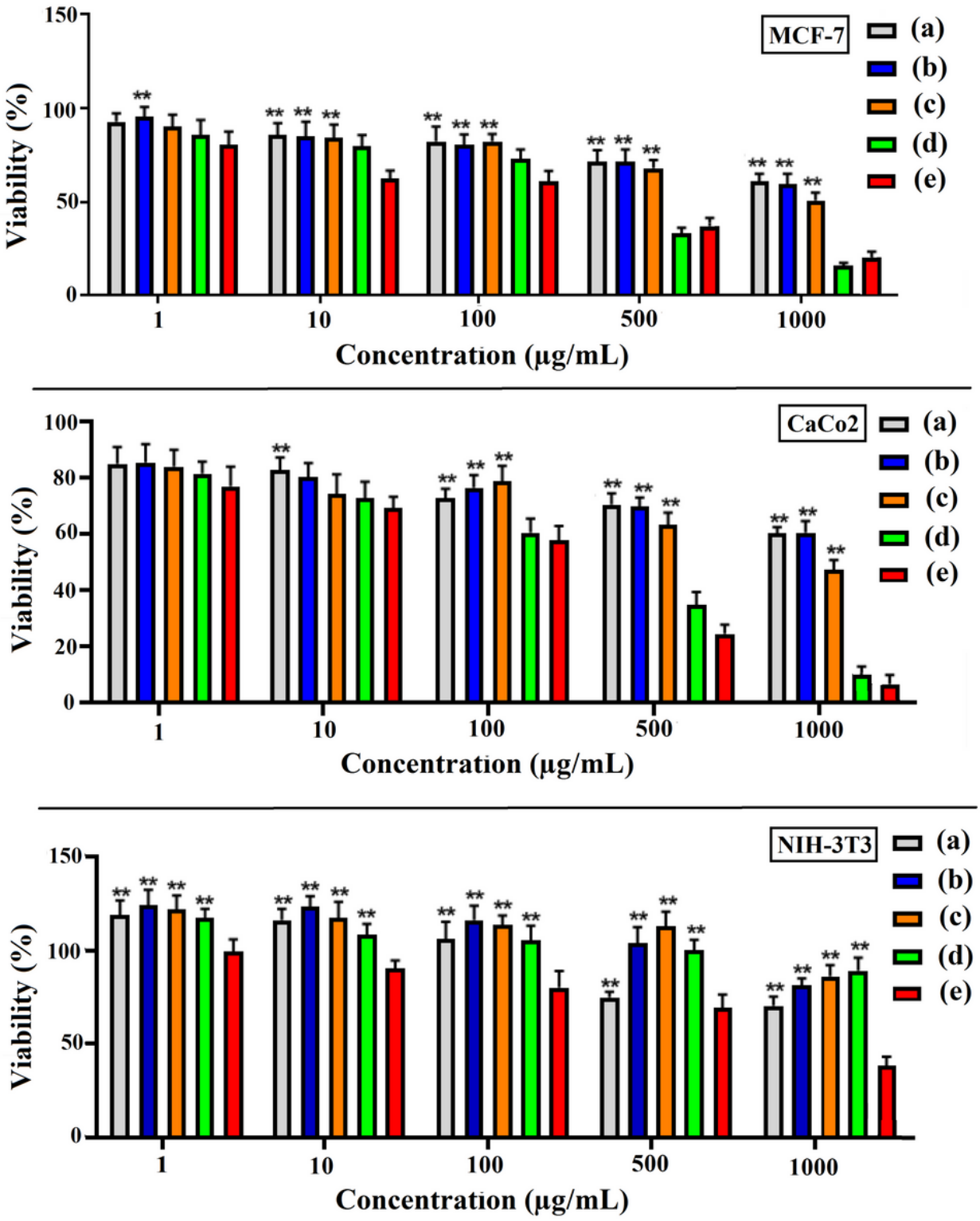

Figure 6

Cell viability of synthesized (a) pure, (b) 1% Co-doped, (c) 4% Co-doped, (d) 8% Co-doped CeO_2 NPs, (e) doxorubicin on MCF-7, CaCo2, and NIH-3T3 cell lines after 24 h incubation.

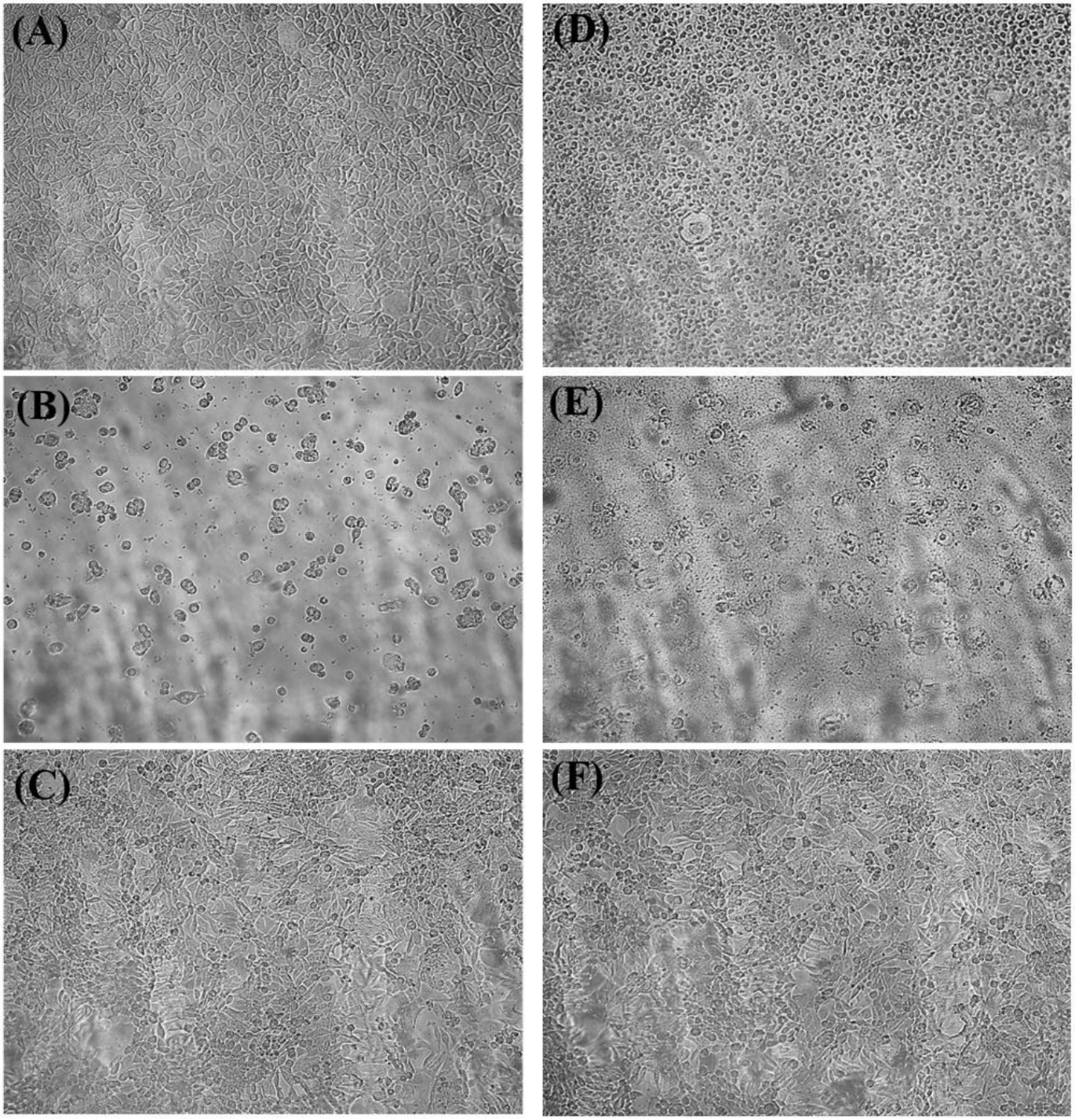

Figure 7

Cell images (A) un-treated MCF-7, (B) un-treated CaCo2, (C) un-treated NIH-3T3, (D) treated MCF-7, (B) treated CaCo2, and (C) treated NIH-3T3 with 8% Co doped CeO_2 NPs